C–C Bond Formation Coupled with C–C Bond Cleavage During Oxidative Upgrading of Glycerol on a Nanoporous $BiVO_4$ Photoanode

Adam M. Hilbrands, McKenna K. Goetz, and Kyoung-Shin Choi*

Department of Chemistry, University of Wisconsin-Madison, Madison, WI 53706, USA

*Correspondence to: kschoi@chem.wisc.edu

Abstract

Production of biodiesel generates glycerol as a 10 wt. % byproduct. Therefore, efficient and selective glycerol upgrading is critical for the sustainable production of biodiesel as well as for the production of chemicals from renewable feedstocks. In this study, the photoelectrochemical glycerol oxidation reaction (GOR) was investigated using a nanoporous $BiVO_4$ photoanode in pH 9.3 and pH 2 buffer solutions. In both solutions, glycolaldehyde (GCAD), a C2 species, was the major product, which has never been the major product in any previous electrochemical or photoelectrochemical GOR study. To produce GCAD from the C3 species glycerol, C–C cleavage should occur to produce C2 and C1 species with a 1:1 ratio. Intriguingly, our results show that during photoelectrochemical GOR on $BiVO_4$, more GCAD is produced than can be explained by simple C–C cleavage, meaning that GCAD is also produced from C–C coupling of two C1 species produced from C–C cleavage. This is equivalent to converting two glycerol molecules to three GCAD molecules, which offers an extraordinary way to maximize GCAD production. To gain further insight into the nature of this unprecedented C–C coupling during GOR, photoelectrochemical oxidation of intermediate oxidation products (glyceraldehyde and 1,3-dihydroxyacetone) and glycerol-1,3-$^{13}C_2$ was compared to that of standard glycerol. Photoelectrochemical GOR was also compared with electrochemical GOR on $BiVO_4$ to interrogate whether light is critical for the observed C–C coupling. Results obtained from comprehensive control experiments revealed critical information about C–C cleavage and C–C coupling during GOR on $BiVO_4$.

Introduction

The need to diversify away from fossil fuels for global energy and chemical production makes the upgrading of biomass an attractive strategy. Increasing production of biodiesel, which can be generated via transesterification of natural plant oils, is a good example of fulfilling this goal. Production of biodiesel, however, generates glycerol as a 10 wt. % byproduct and glycerol production now exceeds millions of tons.[1,2] Thus, utilizing glycerol as a cheap, abundant, and renewable feedstock for chemical production is critical not only for the sustainable production of biodiesel but also for fulfilling the goal of producing chemicals from biomass upgrading.[3,4]

The glycerol oxidation reaction (GOR) can produce various C3-C1 products (**Figure 1**), nearly all of which are more valuable than glycerol.[5–8] Therefore, production of any of these chemicals would be beneficial if it can be achieved selectively and efficiently. Electrochemical and photoelectrochemical GOR are of particular interest as they can be used as the anode reaction coupled with a cathode reaction that produces fuels (e.g., water reduction to H_2, CO_2 reduction to C-based fuels, N_2 reduction to NH_3) in electrochemical and photoelectrochemical fuel production cells.[8–12] While water oxidation has typically been used as the anode reaction in these cells, replacing water oxidation with GOR would allow for the simultaneous production of valuable chemicals at the anode and fuels at the cathode within the same cell, increasing the efficacy of the cell.

When GOR is performed on the photoanode in a photoelectrochemical cell, holes generated in the valence band (VB) of the photoanode are used for glycerol oxidation. Oxide-based photoanodes that tend to have a VBM more positive than 2 V vs RHE[13,14] are of particular interest as they would generate highly oxidizing holes that have sufficient overpotential for GOR without needing the application of a strongly anodic bias as in the case of electrochemical GOR. These highly oxidizing holes would also be thermodynamically capable of performing the oxygen evolution reaction (OER), which may lower the Faradaic efficiency (FE) for GOR. Fortunately, all the oxide-based photoanodes are poorly catalytic for OER and always need an OER catalyst on the surface to utilize surface reaching holes for OER without losing them to surface recombination.[13,14] This means that if a photoanode whose surface is particularly catalytic for GOR is identified, it can achieve GOR with a high FE without requiring an additional GOR catalyst and without losing holes to OER. Thus, the use of GOR instead of OER as the photoanode reaction can also simplify photoanode preparation in addition to producing more valuable chemicals than O_2.

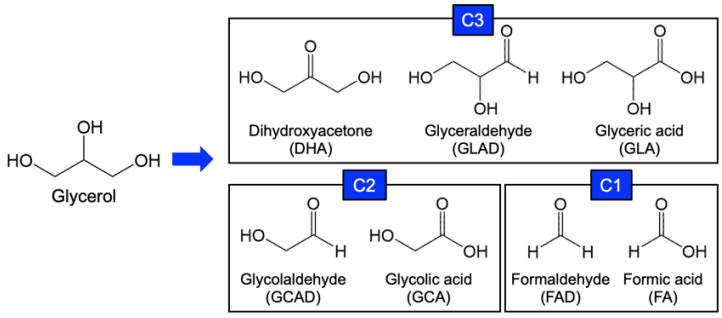

Figure 1. Selected C3, C2, and C1 products from glycerol oxidation.

$BiVO_4$ has been identified as a promising photoanode for GOR. $BiVO_4$ is an n-type semiconductor with a relatively small bandgap (2.4 - 2.5 eV) and can utilize visible light in the solar spectrum for GOR.[15] It has a sufficiently positive VBM (2.4 - 2.5 V vs RHE) that would provide photogenerated holes with a sufficient overpotential to perform GOR. $BiVO_4$ is also known for its exceptional charge separation efficiency,[16,17] meaning it can achieve a higher photon-to-photocurrent conversion efficiency for GOR than other oxide-based photoelectrodes that typically suffer from considerable electron-hole recombination after photon absorption. Additionally, $BiVO_4$ has very poor kinetics for OER.[17,18] Thus, it would be highly advantageous if $BiVO_4$ can perform GOR to produce valuable products selectively and efficiently.

A survey of the previous studies revealed that to date only formic acid (FA) at pH 9[19,20] and 1,3-dihydroxyacetone (DHA) at pH 2[21–23] have been obtained as the major products when photoelectrochemical GOR was performed on $BiVO_4$. It is not clear, however, if the difference in major products in these two pH conditions is solely due to the difference in pH since the $BiVO_4$ photoanodes used in these studies were prepared differently. It is possible that $BiVO_4$ photoanodes prepared by different methods might have different surface compositions, which could have affected their catalytic properties. We also note that some of these studies quantified only the major products, which makes it difficult to gain a comprehensive understanding of all the possible products that can be obtained by GOR on $BiVO_4$ and how the product distribution changes by varying oxidation conditions.

In the current study, we investigated photoelectrochemical GOR at pH 9.3 and pH 2 using the same nanoporous $BiVO_4$ photoanodes and performed a thorough product analysis. To our surprise, the major product obtained from both solutions was glycolaldehyde (GCAD), a C2 species. This species has never been obtained as the major product in any of the previous GOR studies whether GOR was performed electrochemically in the dark or photoelectrochemically under illumination. GCAD has recently shown promise as a starting material for the synthesis of C2 alkanolamines and ethylene diamines[24] which have applications in the synthesis of surfactants,[25] cosmetics,[26] and pharmaceuticals.[27] The use of glycolaldehyde for C2 amine synthesis could replace the commonly used ethylene oxide[28] and dichloroethane, which are more toxic.[29] Additionally, glycolaldehyde has been shown to be a promising platform chemical for the synthesis of tetrose molecules[30,31] that can be used as polymer building blocks.[32] An even more intriguing discovery from our current study is that $BiVO_4$ has the ability to convert two glycerol molecules into three GCAD molecules, which requires not only C–C cleavage of glycerol to form C2 (GCAD) and C1 species but also C–C coupling of two C1 species. While C–C cleavage during GOR is a commonly observed reaction, C–C coupling during GOR has never been reported prior to our work. The conversion of two glycerol molecules to three GCAD molecules offers an extraordinary way to maximize GCAD production from GOR. Here, we report a comprehensive investigation of photoelectrochemical GOR on $BiVO_4$ photoanodes, which produces GCAD as the major product via unprecedented C–C coupling combined with C–C cleavage.

Experimental

Preparation of $BiVO_4$ electrodes Nanoporous $BiVO_4$ electrodes used in this study were prepared using a previously reported method, which is briefly summarized here.[33] A plating solution for the electrodeposition of BiOI was composed of 50 mL water (>18 MΩ cm), 20 mL ethanol (Decon Laboratories 200 proof), 168 μL lactic acid (Alfa Aesar 85%), and 140 μL of 10-

fold diluted HNO_3 (Sigma-Aldrich 70%). This plating solution contained 11 mM $BiNO_3$ (Sigma-Aldrich 98%), 285 mM KI (Sigma-Aldrich 99%), and 13 mM *p*-benzoquinone (Sigma-Aldrich 98%). The final pH of the plating solution was 3.7. A three-electrode setup was used with fluorine-doped tin oxide (FTO) (TEC15, Hartford Glass) as the working electrode (WE), Pt as the counter electrode (CE), and Ag/AgCl (4 M KCl) as the reference electrode (RE). The FTO WE was prepared by washing in soapy water, rinsing with water (>18 MΩ cm), sonicating in acetone (Sigma-Aldrich 99.9%), sonicating in isopropanol (Sigma-Aldrich 99.5%), sonicating in water (>18 MΩ cm), and blow drying with a stream of air. The electrodes were masked with Teflon tape (3M) to expose a 1 cm × 1.2 cm area. In order to electrodeposit BiOI, a potential of –0.32 V vs the Ag/AgCl RE was applied for 20 s to induce Bi nucleation, and then a potential of –0.10 V vs the Ag/AgCl RE was applied to grow a BiOI film while passing a total charge of 0.33 mC/cm^2. The samples were then rinsed with deionized water (>18 MΩ cm) and dried under a stream of air. To convert the BiOI electrode to a $BiVO_4$ electrode, a dimethyl sulfoxide (VWR) solution containing 200 mM $VO(C_5H_7O_2)_2$ (Sigma-Aldrich 98%) was prepared and 65 μL were drop cast onto the 1.2 cm^2 BiOI electrode. The BiOI electrode was then annealed in air at 450 °C for 2 hours to form $BiVO_4$. The resulting electrode was then rinsed in 1 M NaOH (Sigma-Aldrich, 98%) for 30 min to remove excess V_2O_5. A representative X-ray diffraction pattern, scanning electron microscopy image, and absorbance spectrum of the nanoporous $BiVO_4$ electrodes used in this study can be found in **Figure S1**.

Materials characterization The morphology of the electrodes was examined by scanning electron microscopy (SEM) (LEO 1530 microscope, Gemini) at an accelerating voltage of 2 kV. The crystallinity and orientation were confirmed using X-ray diffraction (XRD) (D8 Advance X-ray diffractometer, Bruker) using nickel-filtered copper Kα-radiation with λ = 1.5418 Å. The optical absorbance of the electrodes was measured using a Cary 5000 ultraviolet–visible–near infrared spectrophotometer (Agilent) with an integrating sphere to simultaneously collect reflectance and transmittance from the electrodes.

Solution preparation for GOR and other reactions A pH 2 buffer solution was prepared by adding H_2SO_4 (Sigma-Aldrich, 95-98%) to a 0.5 M Na_2SO_4 (Sigma-Aldrich, >99%) solution to lower the pH to 2. A pH 9.3 buffer solution was prepared by adding NaOH (Sigma-Aldrich, 98%) to a solution containing 0.25 M H_3BO_3 (Sigma-Aldrich, 99.5%) and 0.25 M Na_2SO_4 (Sigma-Aldrich, >99%) to raise the pH to 9.3. We used a solution containing 0.25 M H_3BO_3 and 0.25 M Na_2SO_4 instead of 0.5 M H_3BO_3 to prepare a pH 9.3 buffer solution because the buffer solution prepared from 0.5 M H_3BO_3 was less efficient for GOR in terms of both photocurrent generation and FE for GOR. We confirmed that the product distribution obtained from these two solutions are comparable (**Figure S2**), meaning the presence of sulfate does not affect the relative selectivities of products.

To these buffer solutions, 0.1 M glycerol (Sigma-Aldrich, 99.5%), 0.4 M Na_2SO_3(Sigma-Aldrich 98%), 0.1 M glycerol-1,3-$^{13}C_2$ (Cambridge Isotope Laboratories), 0.1 M DHA (Alfa Aesar), or 0.1 M GLAD (Sigma-Aldrich 90%) was added as needed.

Photoelectrochemical and electrochemical measurements. All photoelectrochemical and electrochemical measurements were performed using an SP-200 potentiostat (Bio-Logic). In order to obtain J-V plots, an undivided 3-electrode cell was used with $BiVO_4$ as the WE, Pt as the CE, and Ag/AgCl (4 M KCl) as the RE. J-t plots were obtained during constant potential

photoelectrolysis and electrolysis under the conditions described below. All potentials were converted to potential versus the reversable hydrogen electrode (RHE) using the following equation (where NHE is normal hydrogen electrode).

$$E(\text{versus RHE}) = E(\text{versus Ag/AgCl}) + E_{Ag/AgCl}(RE) + 0.0591V \times pH$$
$$(E_{Ag/AgCl}(RE) = 0.1976 \text{ V versus NHE at 25 °C}) \quad (1)$$

For photoelectrochemical measurements and photoelectrolysis, simulated solar light was generated using an LCS-100 solar simulator (Oriel Instruments) equipped with a 100 W Xe arc lamp (Newport) and an AM 1.5G filter. An infrared filter (Newport) and a focusing lens were placed between the light source and the electrode. As the light is illuminated through the back side of the $BiVO_4$ electrode, the intensity of light was calibrated to 1 sun (100 mW/cm^2) at the back side of the $BiVO_4$ electrode using a National Renewable Energy Laboratory-certified GaAs reference cell (photovoltaic measurement).[34]

Constant potential (photo)electrolyses were performed using the same three electrode setup described above but in a divided quartz cell with a Nafion 212 cation exchange membrane (Fuel Cell Store). Both the anolyte and catholyte chamber contained 12 mL of solution containing a species to be oxidized. The anolyte was stirred during the (photo)electrolyses. Prior to photoelectrolysis, the $BiVO_4$ electrode was illuminated for 3 min at open circuit potential after which a desired constant potential (0.6 V_{RHE} or 1.0 V_{RHE}) was applied until passing a total charge of 10 C, which is equivalent to ~1 e^- per 10 glycerol (or other organic species) molecules in solution.

For the electrolysis in the dark, the electrolysis setup was placed in a closed box to prevent ambient light from reaching the $BiVO_4$ electrodes. The $BiVO_4$ electrode was at rest for 3 min at open circuit potential and then 1.85 V_{RHE} was applied for the pH 9.3 solution and 2.0 V_{RHE} was applied for the pH 2 solution. Product quantification was performed after 5 C of charge had passed.

Product analysis Quantification of electrolysis products was achieved using high-performance liquid chromatography (HPLC, Prominence-i LC 2030 C 3D, Shimadzu). The mobile phase was 0.1% H_2SO_4 in >18 MΩ cm water and the stationary phase was an ICSep ICE-COREGEL 87H3 column. The flow rate was 0.5 mL/min with a column temperature of 40 °C. Integration of PDA absorbances at multiple wavelengths were compared to calibration curves of all identified products to quantify each product (Details of HPLC quantification and example chromatograms can be found in **Table S1** and **Figure S3**). Quantification of co-eluting peaks was done using unique absorbances and/or solving a system of equations using the integration from multiple wavelengths. Product detection was also verified using ^{1}H NMR (**Figure S4**). NMR spectroscopy was performed using a Bruker Avance III 400MHz NMR spectrometer. Formaldehyde could not be quantified by HPLC, so a comparison of the integration of the formaldehyde ^{1}H NMR peak to the integrations of the ^{1}H NMR peaks of the other products that were quantified using HPLC was used to quantify formaldehyde.

Faradaic efficiency (FE) was calculated for each product using equation 2, where n is the moles formed of that product, z is the number of electrons required to form that product (see SI for z numbers for all products),[35] F is Faraday's constant (96485 C/mol), and Q is the total charge passed.

$$FE\ (\%) = \frac{n \cdot z \cdot F}{Q} \times 100\% \quad (2)$$

Relative selectivity was calculated using equation 3.

$$\text{Relative Selectivity} = \frac{\text{mol of specific product}}{\text{mol of all products detected}} \quad (3)$$

Results and Discussion

Photoelectrochemical GOR on nanoporous $BiVO_4$ We first obtained J-V plots for photoelectrochemical oxidation of water and glycerol using nanoporous $BiVO_4$ photoanodes to compare the catalytic ability of the nanoporous $BiVO_4$ surface for OER and GOR in pH 9.3 borate buffer and pH 2 sulfate buffer solutions with and without 0.1 M glycerol. In both solutions, a considerably higher photocurrent density was obtained with glycerol than without glycerol, suggesting that the nanoporous $BiVO_4$ surface is significantly more catalytic for glycerol oxidation than for water oxidation. In fact, the photocurrent obtained for GOR is almost comparable to the photocurrent obtained with sulfite (**Figure S5**) that is known to be the best hole acceptor with the fastest oxidation kinetics (e.g., almost all surface reaching holes can be used for sulfite oxidation before being lost to surface recombination).[34] This comparison directly shows that holes in the VB of $BiVO_4$ can be efficiently utilized for GOR. This means that a high FE for GOR can be achieved by $BiVO_4$ without adding an additional GOR catalyst on $BiVO_4$.

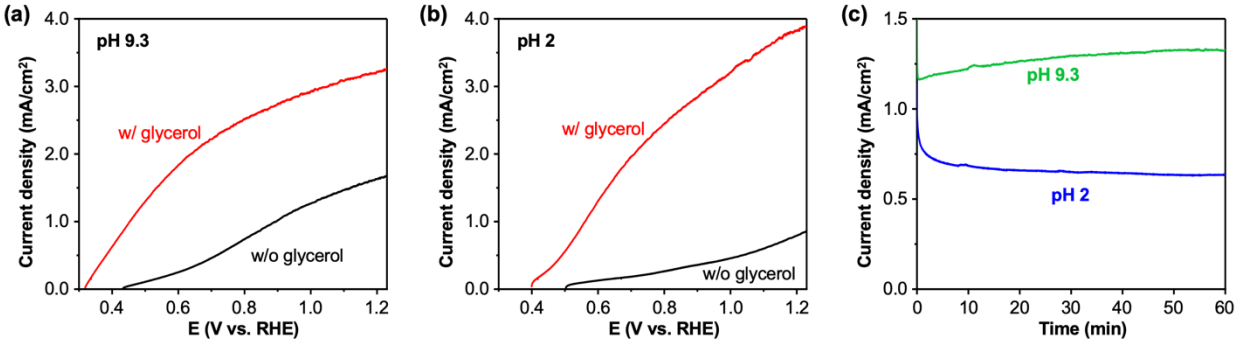

Figure 2. J-V plots of $BiVO_4$ obtained in (a) pH 9.3 and (b) pH 2 buffer solutions with (red) and without (black) 0.1 M glycerol (scan rate 10 mV/s). (c) J-t plots of $BiVO_4$ at 0.6 V_{RHE} in pH 2 (blue) and pH 9.3 (green) buffered solutions containing 0.1 M glycerol. All measurements were performed under AM 1.5G, 100 mW/cm^2 illumination.

Next, a constant potential glycerol oxidation reaction was performed in both pH 9.3 and pH 2 solutions at 0.6 V_{RHE} (V_{RHE} = V vs RHE) under AM 1.5G illumination. The photoelectrolysis was performed for 1 hour in an H-cell divided with a Nafion cation exchange membrane. The J-t plots obtained during the photoelectrolysis are shown in **Figure 2c**. The averaged photocurrent densities were 1.28 mA/cm^2 and 0.67 mA/cm^2 in pH 9.3 and pH 2 solutions, respectively. The $BiVO_4$ photoanodes showed no sign of corrosion after the photoelectrolysis, indicating that long term glycerol photoelectrolysis on $BiVO_4$ is possible. Notably, using bare $BiVO_4$ with no OER catalyst for water oxidation on this timescale normally results in photocorrosion, as surface

reaching holes, which cannot be promptly consumed for OER without a catalyst, are accumulated on the surface and photocorrode the $BiVO_4$ instead.[33] The photostability of $BiVO_4$ for GOR confirms that the rate of GOR is much faster than the photocorrosion rate of $BiVO_4$, and it can kinetically suppress the anodic photocorrosion of $BiVO_4$.

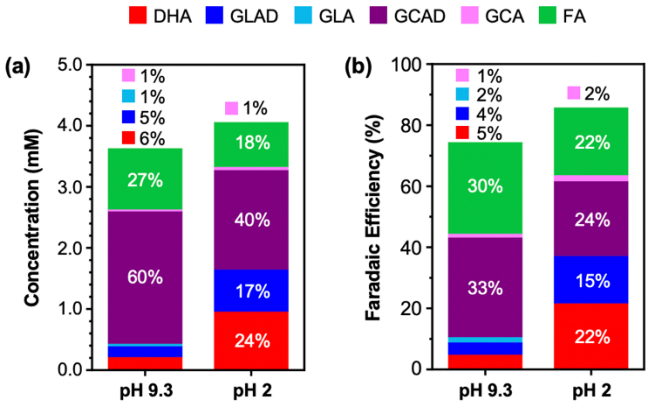

Figure 3. Products obtained from constant potential GOR on $BiVO_4$ at 0.6 V_{RHE} in pH 9.3 and pH 2 buffer solutions containing 0.1 M glycerol after passing 10 C under AM 1.5G, 100 mW/cm^2 illumination; (a) Product concentrations with the relative selectivities shown in the graph and (b) FEs with the exact percentages shown in the graph.

All products obtained from constant potential GOR were quantified and are shown in **Figure 3a**. The number in the bar graph represents the relative selectivity of each product detected. Relative selectivities (which compare a given product amount to the total detected amount of products and neglect stoichiometry) are used instead of the absolute selectivities (which compare a given product amount to the consumed amount of glycerol and consider stoichiometry) to discuss the product distribution because the amount of glycerol consumed during electrolysis is difficult to quantify because glycerol and DHA cannot be adequately separated by HPLC.[35] The FE for each product is shown in **Figure 3b**. The equations used to obtain relative selectivities and FEs for all products are shown in the methods section and the SI.

The major product obtained in a pH 9.3 solution was GCAD, which accounted for 60% of the observed products. To the best of our knowledge, this is the first time that GCAD has been obtained as the major product from GOR whether it was performed photoelectrochemically or electrochemically. FA was detected as the second dominant product. Several other products such as glyceraldehyde (GLAD), glyceric acid (GLA), DHA, and glycolic acid (GCA) were detected but their amounts are negligible (relative selectivity < 7%).

When C–C cleavage of glycerol (C3) occurs to produce C2 and C1 species, the C2:C1 ratio should be 1:1 if no other C–C cleavage reaction occurs (**Figure 4a**). As GCAD and FA are the only C2 and C1 species detected (except for GCA whose relative selectivity is negligible), the GCAD:FA ratio is expected to be 1:1. However, the GCAD:FA ratio shown in **Figure 3a** is ~2.2:1, which deviates considerably from 1:1. As GCAD as well as other C2 species can undergo C–C cleavage to form more FA, the GCAD:FA ratio can be lower than 1:1. A GCAD:FA ratio greater than 1:1 cannot be explained unless we assume that some FA is consumed by further oxidation to CO_2. However, when we considered this possibility and counted the electrons that would be needed

to convert the missing FA to CO_2, the total FE for GOR was calculated to be 137%, far exceeding 100%, suggesting that this scenario alone cannot explain the observed GCAD:FA ratio of ~2.2:1 (see SI for calculation details). Additionally, a control experiment using 0.1 M FA as the starting molecule shows that the kinetics of FA oxidation to CO_2 on $BiVO_4$ is significantly slower than that of glycerol oxidation on $BiVO_4$ under the same oxidation conditions (**Figure S6**), meaning considerable loss of FA as CO_2 is unlikely, especially when the FA concentration in solution during GOR is very low (< 5 mM).

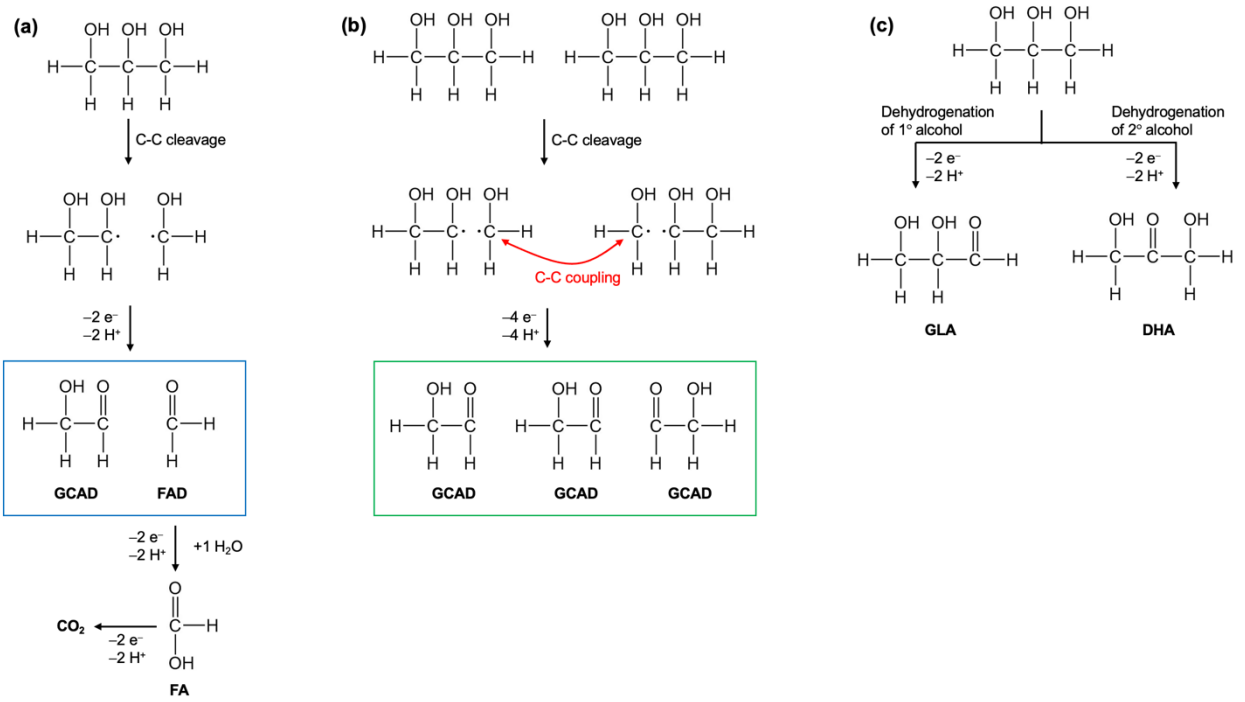

Figure 4. Scheme showing (a) C–C cleavage of glycerol producing a 1:1 ratio of GCAD:FAD (the FAD can be further oxidized to FA) and (b) C–C cleavage of glycerol combined with C–C coupling converting two glycerol to three GCAD without forming FA. In these schemes, C–C cleavage is shown as an initial nonelectrochemical reaction, producing two C radicals, for simplicity. In real GOR, where C–C cleavage occurs under oxidative conditions, C–C cleavage will occur concertedly with the extraction of electrons and protons in various ways. (c) Primary and secondary alcohol oxidation of glycerol producing GLAD and DHA, respectively.

The only other possibility to explain the observed GCAD to FA ratio is that GCAD is formed not only from C–C cleavage of C3 species but also by C–C coupling of two C1 species produced during C–C cleavage. We hypothesize that two C1 species formed from C–C cleavage of two neighboring glycerol molecules on the $BiVO_4$ surface undergo C–C coupling to form GCAD. In other words, three GCAD molecules are formed from two glycerol molecules via C–C coupling as well as C–C cleavage as shown in **Figure 4b**. As this conversion does not involve the formation of FA, and FA can form from other pathways (e.g., C–C cleavage of GCAD and other C2 and C3 species), the GCAD:FA ratio does not need to be 1:1.

In **Figure 4a-b**, C–C cleavage is shown as a nonelectrochemical reaction, producing two C radicals, which is followed by the removal of electrons and protons. However, these two-step representations separating the C–C cleavage step and dehydrogenation step are only for simplicity to make electron and proton count easy. In real GOR, where C–C cleavage is induced under oxidative conditions, C–C cleavage will be oxidative, meaning C–C cleavage and electron extraction will occur in a concerted manner. One such example is shown in **Figure 5a.** Since there are various ways to couple C–C cleavage and the extraction of electrons and protons, the C–C cleavage step is shown as a separate step in the simple two-step representations used in **Figure 4a-b.** We note that C–C coupling under oxidative conditions should also be coupled with electron (and proton) extraction as shown in **Figure 5b**.

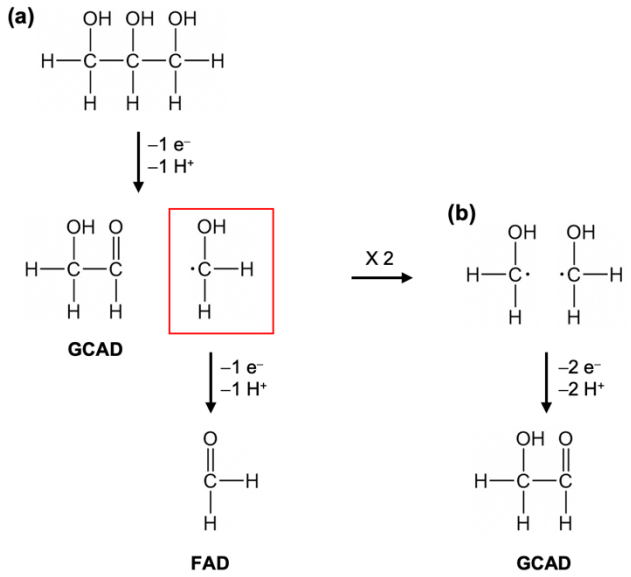

Figure 5. (a) A schematic example showing how C–C cleavage can be coupled with an extraction of an electron/proton pair. The resulting C1 radical can be further oxidized to form a C1 product like FAD or FA or it can undergo C–C coupling to form a C2 species. (b) A schematic showing oxidative C–C coupling where C–C coupling and an extraction of an electron/proton pair occur in a concerted manner.

A similar result was obtained in a pH 2 solution; the major product is also GCAD, which accounts for 40% of the observed products, and the second major product is also FA, which accounts for 18% of the observed products. Again, the GCAD:FA ratio is much higher than 1:1 and attempting to explain the deviation from the 1:1 ratio by counting the electrons required for further oxidation of FA to CO_2 resulted in a 136% FE, greater than 100% FE. The only difference in product distribution between pH 9.3 and pH 2 solutions is that considerably more C3 products (DHA and GLAD) are produced in the pH 2 solution (**Figure 4c**). Control experiments examining the oxidation of DHA and GLAD (discussed below) suggest that the GCAD observed during glycerol oxidation primarily comes from glycerol itself and not from DHA or GLAD. Thus, the fact that more DHA and GLAD and less GCAD are produced at pH 2 suggests that the dehydrogenation rate of glycerol to GLAD and DHA is faster at pH 2 than at pH 9.3, relative to the conversion rate of three glycerol to two GCAD molecules.

We also repeated photoelectrochemical glycerol oxidation at 1.0 V_{RHE} while keeping other conditions the same. As the oxidation potential of holes used for photoelectrochemical GOR is fixed by the valence band edge position, which is not affected by the applied potential, and an application of a more positive potential increases only the number of surface-reaching holes by aiding electron-hole separation, the use of 1.0 V_{RHE} instead of 0.6 V_{RHE} should not alter the product distribution. Indeed, our results show no noticeable changes in the relative selectivities and FEs of products obtained at 0.6 V_{RHE} and at 1.0 V_{RHE} (**Figure S7**).

Understanding C–C coupling to form GCAD While C–C cleavage is a commonly observed reaction during glycerol oxidation,[5,19,20,35] C–C coupling of C1 species during GOR to form C2 products has never been reported previously. Thus, we performed various experiments to increase our understanding of this intriguing reaction. We first examined which C3 species among glycerol, GLAD, and DHA can undergo combined C–C cleavage and C–C coupling to convert two C3 species to three GCAD molecules by using GLAD and DHA as starting molecules. The results obtained from these reactions, summarized in **Table 1**, reveal many interesting features about oxidative C–C cleavage and C–C coupling reactions.

When GLAD was used as the reactant, GCAD and FA were detected in a nearly 1:1 ratio, which is what is expected from simple C–C cleavage of a C3 species resulting in C2 and C1 products (**Figure 6a**). We note that when GLAD undergoes oxidative C–C cleavage, the secondary alcohol is oxidized to an aldehyde and the formal oxidation state of that C increases from 0 to +1. In addition, the terminal aldehyde undergoing C–C cleavage is oxidized to a carboxylic acid and the formal oxidation state of the terminal C increases from +1 to +2. In this case, the resulting C1 species (FA) cannot undergo C–C coupling with another FA to form GCAD under the oxidative condition because C in FA (oxidation state of +2) is more oxidized than C in GCAD (0 on average). This explains why two GLAD molecules cannot be converted to three GCAD molecules.

Table 1. Photoelectrochemical oxidation results on $BiVO_4$ at 0.6 V_{RHE} in pH 9.3 buffer solution containing 0.1 M reactant after 10 C of charge were passed (AM 1.5G illumination).

Reactant	Reactant consumed	GCAD	GCA	FA
GLAD	3.96 mM	3.25 mM	0 mM	3.87 mM
DHA	4.77 mM	2.27 mM	4.05 mM	0.2 mM

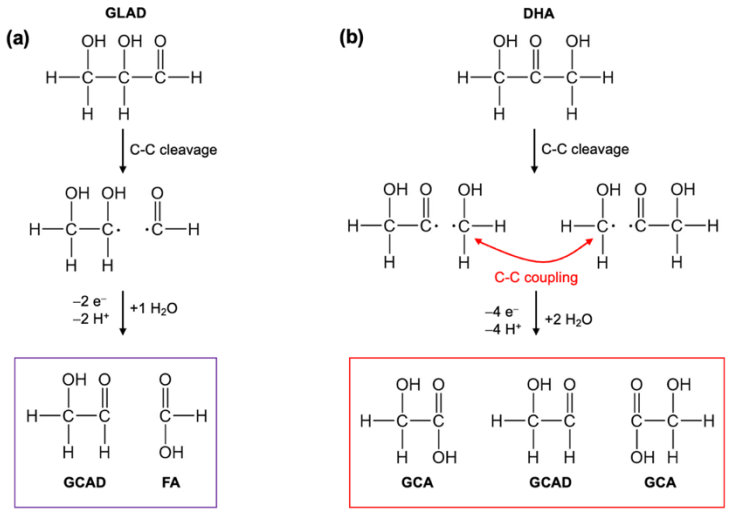

Figure 6. Schemes showing (a) C–C cleavage of GLAD resulting in a 1:1 ratio of GCAD:FA and (b) C–C cleavage combined with C–C coupling of two DHA molecules resulting in a 1:2 ratio of GCAD:GCA.

When DHA is used as the starting molecule, the total amount of C2 species (GCAD and GCA) generated is more than the amount of DHA consumed and negligible FA was detected. These results unambiguously suggest that two DHA molecules are converted to three C2 species. The C2 species produced from DHA oxidation are not just GCAD as in the case of glycerol but GCAD and GCA with a 1:2 ratio. As discussed above in the case of GLAD, C–C cleavage occurring under anodic bias is coupled with oxidation. Therefore, the oxidation states of any C that undergo C–C cleavage must increase after C–C cleavage. Since DHA is a more oxidized species than glycerol, the species that form from the oxidative C–C cleavage of DHA must be more oxidized than those obtained from that of glycerol. The proposed C–C cleavage and C–C coupling reactions of DHA are shown in **Figure 6b**; the central ketone of DHA is oxidized to a carboxylic acid during C–C cleavage, increasing the oxidation state of that C from +2 to +3. As a result, GCA instead of GCAD is produced. On the other hand, the terminal C of DHA and the terminal C of glycerol have the same primary alcohol functional group. Thus, when the terminal C is cleaved from DHA and undergoes C–C coupling with another terminal C cleaved from a neighboring DHA, it forms GCAD, as in the case of glycerol.

The results obtained from GLAD and DHA show that C–C coupling does not occur when GLAD undergoes C–C cleavage and C–C coupling combined with C–C cleavage of DHA generates GCAD and GCA with a 1:2 ratio. As the amount of GCA detected from GOR was negligible, the control experiments with GLAD and DHA suggest that C–C coupling to form GCAD during GOR mainly occurs with C1 species produced from C–C cleavage of glycerol and not of GLAD or DHA. It appears that although DHA is formed from GOR, once DHA desorbs from the photoelectrode surface, DHA cannot compete with glycerol for further oxidation as the glycerol concentration in solution is much higher. Thus, the probability for desorbed DHA to be further oxidized is low.

The understanding that it is two glycerol molecules that undergo combined C–C cleavage and C–C coupling to form three GCAD molecules led to the prediction that if the glycerol concentration increases, the FE for GCAD production should increase further as it would increase the coverage of glycerol on the $BiVO_4$ surface, decrease the distance between the C1 species

generated from C–C cleavage of glycerol, and increase the chance to form GCAD by C–C coupling. Indeed, when we increase the concentration of glycerol from 0.1 M to 1 M, the relative selectivity for GCAD increases from 60% to 73% and the FE increases from 33% to 42% in a pH 9.3 solution (**Figure 7**). On the other hand, when the glycerol concentration is decreased to 0.01 M, OER becomes competitive and the combined FE for GOR decreases considerably (to only ~11%), with the relative selectivity for GCAD decreasing to 47%. These results show that the use of a concentrated glycerol solution is beneficial not only for suppressing OER but also for increasing the relative selectivity and FE for GCAD.

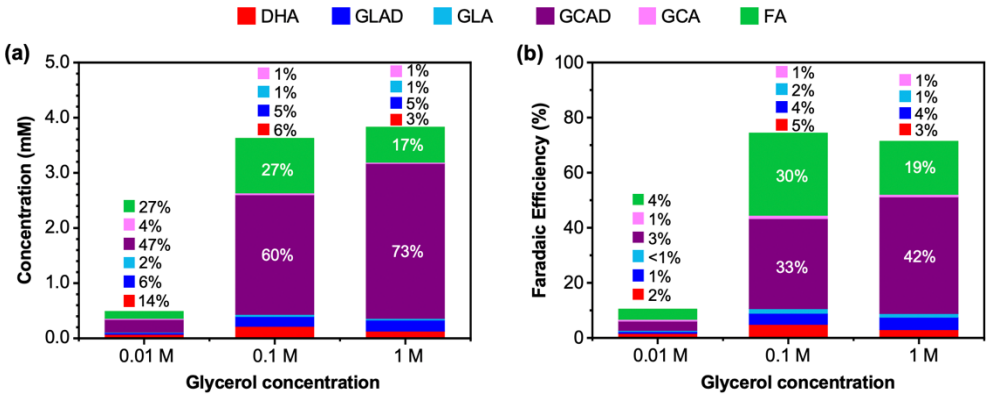

Figure 7. Products obtained from constant potential GOR on $BiVO_4$ at 0.6 V_{RHE} in pH 9.3 buffer solution containing 0.01 M, 0.1 M, and 1 M glycerol after passing 10 C under AM 1.5G, 100 mW/cm^2 illumination; (a) Product concentrations with the relative selectivities shown in the graph and (b) FEs with the exact percentages shown in the graph.

GOR with glycerol-1,3-$^{13}C_2$ We also performed GOR using glycerol-1,3-$^{13}C_2$ in which both primary carbons are labeled with ^{13}C atoms. As we hypothesize that C–C coupling occurs between the primary C of two different glycerol molecules as shown in **Figure 4b**, C–C coupling during the oxidation of glycerol-1,3-$^{13}C_2$ should form some GCAD with both C being ^{13}C atoms, which should be detectable by ^{13}C NMR. Interestingly, however, oxidation of glycerol-1,3-$^{13}C_2$ resulted in a product distribution that is very different from that obtained from the oxidation of standard glycerol (**Figure 8a-b**). First, the amount of GCAD is reduced considerably and the GCAD:C1 ratio is no longer greater than 1:1, meaning there is no reason to believe that C–C coupling occurred with glycerol-1,3-$^{13}C_2$. Second, a significant amount of formaldehyde (FAD) was produced, whereas FAD was not produced with standard glycerol. These results are different from what we originally expected (i.e., formation of GCAD with two ^{13}C atoms), but they make sense when we consider a kinetic isotope effect (KIE) from ^{13}C. The C1 species formed from C–C cleavage of glycerol-1,3-$^{13}C_2$ contains a ^{13}C atom and the rate of C–C coupling involving these heavier ^{13}C atoms is expected to decrease. As C–C coupling is slower, the chance that the C1 species formed from C–C cleavage desorbs from the photoanode surface as FAD increases (**Figure 8c**). As FAD and FA can form by C–C cleavage of GCAD as well as various other C3 and C2 species, detecting more combined C1 species than GCAD is possible. The fact that a sizable amount of FAD is detected with glycerol-1,3-$^{13}C_2$ while FAD was not detected with standard glycerol means that dehydrogenation of FAD containing ^{13}C is slower than that of standard FAD.

Considering that dehydrogenation of aldehydes in aqueous media occurs primarily after an aldehyde is converted to a geminal diol,[36,37] the observed result indicates that the conversion rate of FAD containing ^{13}C to a corresponding geminal diol also slows down with a heavier ^{13}C atom.[38,39]

We note that the GCAD:FAD ratio or the FAD:FA ratio obtained from glycerol-1,3-$^{13}C_2$ oxidation in pH 9.3 and pH 2 are different. This is possible because there are multiple routes to form FAD and FA by C–C cleavage (e.g., C–C cleavage of GCAD and other C3 species) and the kinetics of these reactions forming FAD and FA as well as the kinetics of converting FAD to FA vary differently with pH.

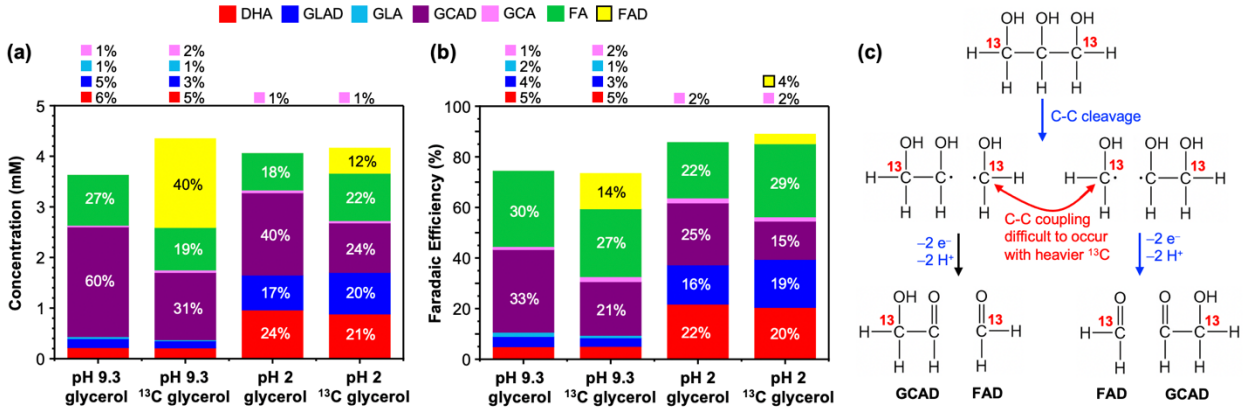

Figure 8. Products obtained from constant potential GOR on $BiVO_4$ at 0.6 V_{RHE} in pH 9.3 and pH 2 buffer solutions containing 0.1 M standard glycerol and glycerol-1,3-$^{13}C_2$ after passing 10 C under AM 1.5G, 100 mW/cm^2 illumination; (a) Product concentrations with the relative selectivities shown in the graph and (b) FEs with the exact percentages shown in the graph. (c) Scheme showing C–C bond cleavage of glycerol-1,3-$^{13}C_2$ where the heavier ^{13}C inhibits C–C coupling, resulting in GCAD and FAD as products.

Electrochemical vs photoelectrochemical GOR on nanoporous $BiVO_4$ The last question we wanted to answer to better understand C–C coupling is if C–C coupling occurs only photoelectrochemically under illumination on $BiVO_4$ or if it can occur electrochemically on $BiVO_4$ in the dark. If it is the former, it means that light or the combination of light and the $BiVO_4$ surface are needed to induce C–C coupling. If it is the latter, it means that the surface of nanoporous $BiVO_4$ used in this study has a special capability to promote C–C coupling (e.g., by stabilizing C1 radical species resulting from C–C cleavage on the surface as a surface bound radical, which increases its chance to undergo C–C coupling with other surface bound C1 species) with or without light.

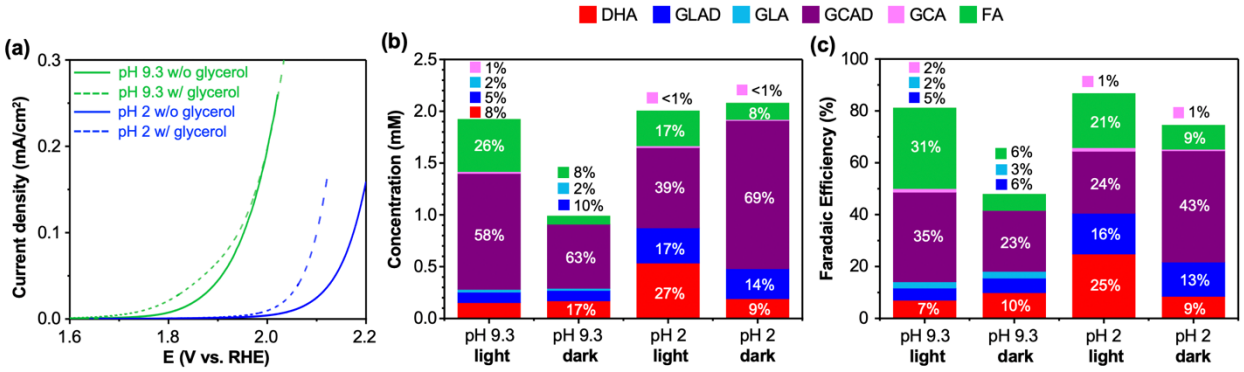

Figure 9. (a) J-V plot of $BiVO_4$ obtained in pH 9.3 (green) and pH 2 (blue) buffer solutions with (dashed) and without (solid) 0.1 M glycerol in the dark. Products obtained from constant potential GOR on $BiVO_4$ in the dark obtained in pH 9.3 (at 1.85 V_{RHE}) and pH 2 (at 2.0 V_{RHE}) buffer solutions after passing 5 C; (b) Product concentrations with the relative selectivities shown in the graph. (c) FEs with the exact percentages shown in the graph. The results obtained from the same solutions at 0.6 V_{RHE} under AM 1.5G, 100 mW/cm^2 illumination after passing 5 C are also shown for comparison.

The LSVs obtained for electrochemical GOR using the same $BiVO_4$ electrode in the dark are shown in **Figure 9a**. Electrochemical GOR on $BiVO_4$ requires the application of highly oxidizing potentials, comparable to those of photogenerated holes in the VB of $BiVO_4$ (~2.4 V vs. RHE). The onset potentials of GOR are 1.60 V_{RHE} and 1.85 V_{RHE} at pH 9.3 and pH 2, respectively. We performed electrochemical GOR in the dark at 1.85 V_{RHE} and 2.0 V_{RHE} at pH 9.3 and pH 2, respectively; at these potentials sufficient anodic current densities could be generated without overwhelming contribution from OER. The product analyses are shown in **Figure 9b-c**. The results show that the GCAD:C1 ratios obtained in the dark are 7.9:1 and 8.6:1 at pH 9.3 and pH 2, respectively, both of which are far from 1:1. Attempting to explain the deviation from the 1:1 ratio by counting the electrons required for further oxidation of FA to CO_2 resulted in combined FEs for GOR of 119% and 208% at pH 9.3 and at pH 2, respectively. These results unambiguously confirm that C–C coupling occurs in the dark as well as under illumination, meaning that the nanoporous $BiVO_4$ used in this study can promote C–C coupling with and without light. The use of $BiVO_4$ as a photoanode under illumination, however, has the advantage of shifting the onset potential for glycerol oxidation to the negative direction by more than 1 V and generating considerably higher current densities for glycerol oxidation (**Figure 2a-b** vs **Figure 9a**). The exact mechanism of how the nanoporous $BiVO_4$ used in this study can facilitate C–C coupling will require further studies, but the current study discovered and confirmed unprecedented C–C coupling during GOR on nanoporous $BiVO_4$ electrodes using various comprehensive control experiments.

Conclusions

In summary, we have investigated photoelectrochemical GOR using an n-type $BiVO_4$ electrode as a photoanode in pH 9.3 and pH 2 buffer solutions. The major product obtained from both solutions is GCAD, which has never been obtained as the major product in any previous GOR study. We also discovered that GCAD is produced not only by C–C cleavage of glycerol but also by C–C coupling of two C1 species produced from C–C cleavage of glycerol, meaning that two

glycerol molecules can be converted to three GCAD molecules. While C–C cleavage during GOR is a commonly observed reaction, C–C coupling during GOR has never been reported prior to our work. Our results show that among C3 species (glycerol, GLAD, and DHA), only glycerol and DHA with both terminal C atoms having an alcohol group can produce C1 species by C–C cleavage that can undergo oxidative C–C coupling to form GCAD. On the other hand, C–C cleavage of GLAD occurs between the secondary alcohol and the aldehyde. The already more oxidized aldehyde group cannot undergo oxidative C–C coupling to produce GCAD and is converted to FA instead. We also show that C–C coupling is suppressed when glycerol-1,3-$^{13}C_2$ is used due to the KIE from the heavier ^{13}C-labeled C1 species generated during C–C cleavage that slow down the C–C coupling reaction. Illumination was found to not be critical for the conversion of two glycerol molecules to three GCAD molecules on $BiVO_4$, which suggests that the surface of $BiVO_4$ used in this study has a special capability to promote C–C coupling. However, a considerably more positive potential needs to be applied to induce electrochemical GOR on $BiVO_4$ in the dark, highlighting the advantage of photoelectrochemical GOR on $BiVO_4$ utilizing highly oxidizing photogenerated holes in the VB of $BiVO_4$. This study shows that the unprecedented ability of $BiVO_4$ to perform combined C–C cleavage and C–C coupling during GOR provides a remarkable way to maximize GCAD production from GOR.

Associated Content

Supporting Information

The Supporting Information is available free of charge at pubs.acs.org

Characterization of $BiVO_4$ electrodes, additional J-V and J-t plots, photoelectrochemical GOR at 1.0 V_{RHE}, FE calculation details, HPLC analysis details and chromatograms, and an NMR spectrum (PDF)

Acknowledgements

This work was supported by the National Science Foundation (NSF) under grant no. CHE-2054986.

Author Information

The authors declare no competing interests.

References

(1) Quispe, C. A. G.; Coronado, C. J. R.; Carvalho Jr., J. A. Glycerol: Production, Consumption, Prices, Characterization and New Trends in Combustion. *Renew. Sust. Energ. Rev.* **2013**, *27*, 475–493.

(2) Anuar, M. R.; Abdullah, A. Z. Challenges in Biodiesel Industry with Regards to Feedstock, Environmental, Social and Sustainability Issues: A Critical Review. *Renew. Sust. Energ. Rev.* **2016**, *58*, 208–223.

(3) Luo, H.; Barrio, J.; Sunny, N.; Li, A.; Steier, L.; Shah, N.; Stephens, I. E. L.; Titirici, M.-M. Progress and Perspectives in Photo- and Electrochemical-Oxidation of Biomass for Sustainable Chemicals and Hydrogen Production. *Adv. Energy Mater.* **2021**, *11*, 2101180.

(4) Dodekatos, G.; Schünemann, S.; Tüysüz, H. Recent Advances in Thermo-, Photo-, and Electrocatalytic Glycerol Oxidation. *ACS Catal.* **2018**, *8*, 6301–6333.

(5) Fan, L.; Liu, B.; Liu, X.; Senthilkumar, N.; Wang, G.; Wen, Z. Recent Progress in Electrocatalytic Glycerol Oxidation. *Energy Technol.* **2021**, *9*, 2000804.

(6) Katryniok, B.; Kimura, H.; Skrzyńska, E.; Girardon, J.-S.; Fongarland, P.; Capron, M.; Ducoulombier, R.; Mimura, N.; Paul, S.; Dumeignil, F. Selective Catalytic Oxidation of Glycerol: Perspectives for High Value Chemicals. *Green Chem.* **2011**, *13*, 1960–1979.

(7) Coutanceau, C.; Baranton, S.; Kouamé, R. S. B. Selective Electrooxidation of Glycerol Into Value-Added Chemicals: A Short Overview. *Front. Chem.* **2019**, *7*, 100.

(8) Wu, J.; Yang, X.; Gong, M. Recent Advances in Glycerol Valorization via Electrooxidation: Catalyst, Mechanism and Device. *Chinese J. Catal.* **2022**, *43*, 2966–2986.

(9) Cha, H. G.; Choi, K.-S. Combined Biomass Valorization and Hydrogen Production in a Photoelectrochemical Cell. *Nat. Chem.* **2015**, *7*, 328–333.

(10) Bender, M. T.; Yuan, X.; Choi, K.-S. Alcohol Oxidation as Alternative Anode Reactions Paired with (Photo)Electrochemical Fuel Production Reactions. *Nat. Commun.* **2020**, *11*, 4594.

(11) Jiang, N.; You, B.; Boonstra, R.; Terrero Rodriguez, I. M.; Sun, Y. Integrating Electrocatalytic 5-Hydroxymethylfurfural Oxidation and Hydrogen Production via Co–P-Derived Electrocatalysts. *ACS Energy Lett.* **2016**, *1*, 386–390.

(12) Jiang, N.; Liu, X.; Dong, J.; You, B.; Liu, X.; Sun, Y. Electrocatalysis of Furfural Oxidation Coupled with H_2 Evolution via Nickel-Based Electrocatalysts in Water. *ChemNanoMat.* **2017**, *3*, 491–495.

(13) Sivula, K.; van de Krol, R. Semiconducting Materials for Photoelectrochemical Energy Conversion. *Nat. Rev. Mater.* **2016**, *1*, 1–16.

(14) Lee, D. K.; Lee, D.; Lumley, M. A.; Choi, K.-S. Progress on Ternary Oxide-Based Photoanodes for Use in Photoelectrochemical Cells for Solar Water Splitting. *Chem. Soc. Rev.* **2019**, *48*, 2126–2157.

(15) Park, Y.; McDonald, K. J.; Choi, K.-S. Progress in Bismuth Vanadate Photoanodes for Use in Solar Water Oxidation. *Chem. Soc. Rev.* **2013**, *42*, 2321–2337.

(16) Kim, T. W.; Ping, Y.; Galli, G. A.; Choi, K.-S. Simultaneous Enhancements in Photon Absorption and Charge Transport of Bismuth Vanadate Photoanodes for Solar Water Splitting. *Nat. Commun.* **2015**, *6*, 8769.

(17) Kim, T. W.; Choi, K.-S. Nanoporous $BiVO_4$ Photoanodes with Dual-Layer Oxygen Evolution Catalysts for Solar Water Splitting. *Science* **2014**, *343*, 990–994.

(18) Seabold, J. A.; Choi, K.-S. Efficient and Stable Photo-Oxidation of Water by a Bismuth Vanadate Photoanode Coupled with an Iron Oxyhydroxide Oxygen Evolution Catalyst. *J. Am. Chem. Soc.* **2012**, *134*, 2186–2192.
(19) Huang, L.-W.; Vo, T.-G.; Chiang, C.-Y. Converting Glycerol Aqueous Solution to Hydrogen Energy and Dihydroxyacetone by the $BiVO_4$ Photoelectrochemical Cell. *Electrochim. Acta* **2019**, *322*, 134725.
(20) Wu, Y.-H.; A. Kuznetsov, D.; C. Pflug, N.; Fedorov, A.; R. Müller, C. Solar-Driven Valorisation of Glycerol on $BiVO_4$ Photoanodes: Effect of Co-Catalyst and Reaction Media on Reaction Selectivity. *J. Mater. Chem. A* **2021**, *9*, 6252–6260.
(21) Liu, D.; Liu, J.-C.; Cai, W.; Ma, J.; Yang, H. B.; Xiao, H.; Li, J.; Xiong, Y.; Huang, Y.; Liu, B. Selective Photoelectrochemical Oxidation of Glycerol to High Value-Added Dihydroxyacetone. *Nat. Commun.* **2019**, *10*, 1–8.
(22) Vo, T.-G.; Kao, C.-C.; Kuo, J.-L.; Chiu, C.; Chiang, C.-Y. Unveiling the Crystallographic Facet Dependence of the Photoelectrochemical Glycerol Oxidation on Bismuth Vanadate. *Appl. Catal. B* **2020**, *278*, 119303.
(23) Tateno, H.; Chen, S.-Y.; Miseki, Y.; Nakajima, T.; Mochizuki, T.; Sayama, K. Photoelectrochemical Oxidation of Glycerol to Dihydroxyacetone Over an Acid-Resistant Ta:$BiVO_4$ Photoanode. *ACS Sustain. Chem. Eng.* **2022**, *10*, 7586–7594.
(24) Faveere, W.; Mihaylov, T.; Pelckmans, M.; Moonen, K.; Gillis-D'Hamers, F.; Bosschaerts, R.; Pierloot, K.; Sels, B. F. Glycolaldehyde as a Bio-Based C2 Platform Chemical: Catalytic Reductive Amination of Vicinal Hydroxyl Aldehydes. *ACS Catal.* **2020**, *10*, 391–404.
(25) Han, B.; Geng, T.; Jiang, Y.; Ju, H. Synthesis and Properties of Di-Chain Esterquat Surfactants. *J. Surfactants Deterg.* **2015**, *18*, 91–95.
(26) Bremecker, K.-D.; Natonski, J. l.; Eachus, A. c. The Role of Primary Alkanolamines in Cosmetic Formulation. *Int. J. Cosmet. Sci.* **1991**, *13*, 235–247.
(27) Calignano, A.; La Rana, G.; Piomelli, D. Antinociceptive Activity of the Endogenous Fatty Acid Amide, Palmitylethanolamide. *Eur. J. Pharmacol.* **2001**, *419*, 191–198.
(28) Lorenti Garcia, C.; Darroudi, F.; Tates, A. D.; Natarajan, A. T. Induction and Persistence of Micronuclei, Sister-Chromatid Exchanges and Chromosomal Aberrations in Splenocytes and Bone-Marrow Cells of Rats Exposed to Ethylene Oxide. *Mutat. Res. Genet. Toxicol. Environ. Mutagen.* **2001**, *492*, 59–67.
(29) Murphy, M. J.; Dunbar, D. A.; Kaminsky, L. S. Acute Toxicity of Fluorinated Ether Anesthetics: Role of 2,2,2-Trifluoroethanol and Other Metabolites. *Toxicol. Appl. Pharmacol.* **1983**, *71*, 84–92.
(30) Tolborg, S.; Meier, S.; Saravanamurugan, S.; Fristrup, P.; Taarning, E.; Sádaba, I. Shape-Selective Valorization of Biomass-Derived Glycolaldehyde Using Tin-Containing Zeolites. *ChemSusChem* **2016**, *9*, 3054–3061.
(31) Dusselier, M.; Van Wouwe, P.; De Smet, S.; De Clercq, R.; Verbelen, L.; Van Puyvelde, P.; Du Prez, F. E.; Sels, B. F. Toward Functional Polyester Building Blocks from Renewable Glycolaldehyde with Sn Cascade Catalysis. *ACS Catal.* **2013**, *3*, 1786–1800.
(32) Dusselier, M.; Van Wouwe, P.; de Clippel, F.; Dijkmans, J.; Gammon, D. W.; Sels, B. F. Mechanistic Insight into the Conversion of Tetrose Sugars to Novel α-Hydroxy Acid Platform Molecules. *ChemCatChem* **2013**, *5*, 569–575.
(33) Lee, D. K.; Choi, K.-S. Enhancing Long-Term Photostability of $BiVO_4$ Photoanodes for Solar Water Splitting by Tuning Electrolyte Composition. *Nat. Energy* **2018**, *3*, 53–60.

(34) Govindaraju, G. V.; Wheeler, G. P.; Lee, D.; Choi, K.-S. Methods for Electrochemical Synthesis and Photoelectrochemical Characterization for Photoelectrodes. *Chem. Mater.* **2017**, *29*, 355–370.
(35) Goetz, M. K.; Bender, M. T.; Choi, K.-S. Predictive Control of Selective Secondary Alcohol Oxidation of Glycerol on NiOOH. *Nat. Commun.* **2022**, *13*, 5848.
(36) Bender, M. T.; Lam, Y. C.; Hammes-Schiffer, S.; Choi, K.-S. Unraveling Two Pathways for Electrochemical Alcohol and Aldehyde Oxidation on NiOOH. *J. Am. Chem. Soc.* **2020**, *142*, 21538–21547.
(37) Bender, M. T.; Choi, K.-S. Electrochemical Dehydrogenation Pathways of Amines to Nitriles on NiOOH. *JACS Au* **2022**, *2*, 1169–1180.
(38) Marlier, J. F. Heavy-Atom Isotope Effects on the Alkaline Hydrolysis of Methyl Formate: The Role of Hydroxide Ion in Ester Hydrolysis. *J. Am. Chem. Soc.* **1993**, *115*, 5953–5956.
(39) Marlier, J. F.; Dopke, N. C.; Johnstone, K. R.; Wirdzig, T. J. A Heavy-Atom Isotope Effect Study of the Hydrolysis of Formamide. *J. Am. Chem. Soc.* **1999**, *121*, 4356–4363.

TOC Graphic